



Search for Randall-Sundrum Gravitons in Dilepton and Diphoton Final States with 1 fb^{-1} of Data

Amitabha Das, Ulrich Heintz

Boston University
(Dated: February 28, 2008)

We report results from a search for the lightest Kaluza-Klein mode of the graviton in the Randall-Sundrum model with a warped extra dimension in 1 fb^{-1} of data from $p\bar{p}$ -collisions at $\sqrt{s} = 1.96 \text{ TeV}$, collected by the DØ detector at the Fermilab Tevatron between October 2002 and February 2006. We search for resonances in the invariant mass spectrum of two electromagnetic showers originating from the decay of the graviton to electron-positron or photon pairs. We set 95% confidence level upper limits on the production cross section times branching fraction into electron-positron pairs of these graviton modes between 51 fb and 2.3 fb for masses of 200 GeV and over 900 GeV, respectively. These translate into lower limits on the mass M_1 of the lightest Kaluza-Klein mode of the graviton of 303 GeV to 898 GeV for couplings of the graviton to standard model fields $\kappa/\overline{M}_{Pl} = 0.01$ to 0.1.

I. THE RANDALL-SUNDRUM MODEL OF EXTRA DIMENSIONS

The standard model has been a great success in explaining all experimental observations in particle physics. Nearly every feature of this theory has been confirmed by experimental results. However, we also know that it has fundamental problems.

Electroweak symmetry breaking is achieved by the Higgs mechanism in the standard model which in its simplest form gives rise to a fundamental scalar of unknown mass, the Higgs boson. This particle has not been observed yet but present experimental data suggest that its mass is between about 115 and 250 GeV if the standard model is correct.

Ultimately we hope to be able to formulate a theory that includes all fundamental interactions including gravity. This would introduce an energy scale much larger than the electroweak scale into the theory and the mass of a fundamental scalar would receive large radiative corrections, driving it up towards the Planck mass. This is called the hierarchy problem. In order to stabilize the mass of the Higgs boson we either need an incredible amount of fine tuning or new physics beyond the standard model that sets in at an energy scale of a few TeV.

The model proposed by Randall and Sundrum[1] postulates the existence of an additional spatial dimension. In addition to the conventional (3+1)-dimensional space, there is a hidden brane (Planck brane) on which gravity is localized. As one moves away from this Planck brane gravity is exponentially suppressed. Hence gravity appears so weak at the standard model brane.

In the simplest RS model, the only particles that propagate in the extra dimension are gravitons. They appear as a Kaluza-Klein (KK) tower of massive excitations. The first excited mode of the graviton could be produced resonantly at the Tevatron. The masses and widths of the KK-excitations are related to the parameters of the RS model. These parameters are expressed in terms of two direct observables: the mass of the first excited mode of the graviton, M_1 and the dimensionless coupling to the standard model fields, κ/\overline{M}_{Pl} which is expected to be within 0.01 and 0.1. The lower bound on the coupling (0.01) comes from a string theory argument[2]. The upper bound (0.1) comes from the constraint on the curvature of the extra dimension[3].

These gravitons can decay into fermion-antifermion or diboson pairs. We search for the lowest excited graviton state as a resonance in the $e^+e^-/\gamma\gamma$ invariant mass spectrum. The branching fraction to $\gamma\gamma$ is twice that to e^+e^- ($B(G \rightarrow \gamma\gamma) = 2 \times B(G \rightarrow e^+e^-)$). We look for decays to e^+e^- and $\gamma\gamma$ final states. These final states have similar signatures in our detector and can thus be treated together.

II. ANALYSIS OVERVIEW

In this paper we report results from a search for Randall-Sundrum (RS) gravitons approximately 1 fb⁻¹ data collected with the DØ detector at Fermilab. DØ has previously published a similar analysis based on 275 pb⁻¹[4] and CDF has preliminary results from a similar search[5].

Our search is based on events with two energy clusters in the calorimeter that are consistent with electromagnetic (em) showers originating from electrons, positrons, or photons produced in the proton-antiproton collision. Graviton decays would appear as a resonance in the invariant mass spectrum of the em cluster pair. We restrict our search to events in which both em showers are in the central calorimeter because there is little or no gain in acceptance for decay products of massive gravitons by including showers in the end calorimeters.

The irreducible background processes that contribute to this data sample are the Drell-Yan (DY) process (e^+e^- production through an intermediate photon or Z boson and prompt di-photon ($\gamma\gamma$) production. We fix the relative normalization of these two processes using their standard-model cross sections. Further backgrounds originate from photon+jet or multijet production in which one or more jets are misidentified as electrons or photons. We call the latter instrumental background. This background is modeled using control data samples. We fix the background model by fitting the spectrum in the mass region around the Z peak to a combination of irreducible background and instrumental background. In this way we make ourselves insensitive to the k-factor for these processes. We will use k-factors to scale the cross sections to next-to-leading order (NLO). However this only affects the value of the integrated luminosity quoted since one would expect that the k-factors scale similarly in going from NLO to NNLO for all these processes. Any uncertainty in the k-factor will therefore cancel in the final cross section limits.

Once the background model is fixed, we count events inside mass windows centered on hypothesized values of M_1 and compare the observed number of events to the background model prediction. We compute an Bayesian upper limit on the production cross section times branching fraction into e^+e^- for the lowest excited graviton state. We study various possible sources of systematic uncertainties and evaluate their sizes

Finally we compare the cross section limits to predictions from the RS model to determine the regions in the model parameters κ and M_1 that we can exclude.

III. COLLIDER DATA AND MONTE CARLO SAMPLES

The data used for this analysis were taken between October 2002 and February 2006. All the data have been reconstructed with version p17 of the $D\bar{O}$ reconstruction program. The starting point for this analysis is the data set with two high- p_T electromagnetic clusters, the so-called “2EMhighpt skim” that consists of approximately 34M events. It was further reduced with the following preselection:

- remove bad runs and bad luminosity blocks
- pass the logical or of a set of eight triggers requiring one or two electromagnetic clusters as listed in Table VIII
- remove duplicate events
- select events with two electromagnetic objects that both satisfy the following loose cuts:
 - ID = 10 or 11
 - $|\text{detector } \eta| < 1.1$
 - $p_T > 25$ GeV
 - fraction of energy in electromagnetic calorimeter $f_{EM} > 0.9$
 - fraction of energy in isolation cone $\frac{E_{Tot}(0.4) - E_{EM}(0.2)}{E_{EM}(0.2)} = f_{iso} < 0.2$

We do not exclude electromagnetic objects near ϕ -boundaries of modules in CC. After these cuts about 1.4M events remain.

Monte Carlo (MC) samples of Drell-Yan (DY) production of e^+e^- final states and direct production of $\gamma\gamma$ final states were used. The DY MC CAF (Common Analysis Format) trees were obtained from the official Common Samples Group summer MC samples generated with PYTHIA [6] in four different mass windows. The $\gamma\gamma$ MC samples were generated with PYTHIA in four different mass windows as well. The details of the different samples along with their leading order (LO) cross sections are listed in Table I. MC samples of RS gravitons were also generated with PYTHIA for different values of the graviton mass and a coupling $\kappa/\overline{M}_{Pl} = 0.1$ with both the final states e^+e^- and $\gamma\gamma$ allowed. The details are listed in Table II.

Process	Mass Window (GeV)	LO Cross-Section (pb)	Number of Events
DY	60-130	178	264750
	130-250	1.3	27500
	250-500	0.11	27000
	>500	0.0045	25500
$\gamma\gamma$	50-130	42.7	50500
	130-250	3.1	51500
	250-500	0.49	26750
	>500	0.034	25500

TABLE I: List of DY and $\gamma\gamma$ MC samples used in this analysis.

IV. EVENT SELECTION

For this analysis events were selected that have two high p_T objects consistent with electromagnetic showers. In order to accept both $\gamma\gamma$ and ee decay channels no track match was required for the objects. The following set of cuts defines an electromagnetic shower for the final event selection:

- ID = 10 or 11
- $|\text{detector } \eta| < 1.1$
- $p_T > 25$ GeV

RS Graviton Mass (GeV)	LO Cross-Section \times Branching Ratio $p\bar{p} \rightarrow G + X, G \rightarrow e^+e^-$ or $\gamma\gamma$ (pb)	Number of Events
200	28.7	10000
220	17.6	10000
240	11.6	10000
250	9.9	10000
270	6.7	10000
300	4.2	10000
320	3.1	10000
350	2.0	10000
370	1.5	10000
400	1.1	10000
450	0.58	10000
500	0.33	10000
550	0.19	10000
600	0.12	10000
650	0.07	10000
700	0.041	10000
750	0.025	10000
800	0.015	10000
850	0.0087	10000
900	0.0051	10000
950	0.0029	10000
1000	0.0016	10000

TABLE II: List of RS graviton MC samples used for this analysis.

- fraction of energy in electromagnetic calorimeter $f_{EM} > 0.97$
- fraction of energy in isolation cone $f_{iso} < 0.07$
- consistency with electromagnetic shower shape : 7×7 H-matrix $\chi^2 < 12$
- sum of transverse momenta (p_T) of tracks in isolation cone ($0.05 < \Delta R = \sqrt{(\Delta\eta)^2 + (\Delta\phi)^2} < 0.4$ around the object direction) $p_{iso} < 2$ GeV

V. BACKGROUND ESTIMATION

The total background is made up of physics backgrounds with genuine e^+e^- and $\gamma\gamma$ final states and instrumental backgrounds in which one or both of the electromagnetic objects are misidentified.

The sources of physics backgrounds are Drell-Yan production of e^+e^- and direct $\gamma\gamma$ production. The contribution from physics background is estimated from the MC samples. In order to predict the shape of the invariant mass spectrum from the physics backgrounds, the spectra from the four Drell-Yan and the four $\gamma\gamma$ MC samples are added according to their NLO cross sections. The NLO cross-section is obtained by multiplying the LO cross-section (Table I) by a mass independent k-factor of 1.34[8]. Here is a detailed description of how the total invariant mass spectrum is made for Drell-Yan MC:

- Apply the full selection cuts to each of the four Drell-Yan MC samples.
- For each sample, fill two sets of invariant mass plots for the selected events.
 - Low mass spectra with invariant mass between 50 and 250 GeV with a bin size of 1 GeV.
 - Full mass spectra with invariant mass between 50 GeV and 1000 GeV with a bin size of 10 GeV.

- The mass spectrum for each MC sample (e.g. Drell-Yan MC sample with mass $60 < M < 130$ GeV) is scaled to the event yield expected from a fixed integrated luminosity using the corresponding NLO cross-section (e.g. $178 \text{ pb} \times 1.34/N_{MC}$). Here $N_{MC} = 264750$ is the number of generated MC events (Table I).
- All the four MC samples are individually scaled in this way and then added to get the Drell-Yan background shape.

Similarly, the direct diphoton background shape is also obtained. Then the Drell-Yan and diphoton total mass spectra are added to get the total physics background shape.

The instrumental background is estimated from a sub sample of the preselected data sample from section III in which at least one electromagnetic object is inconsistent with an electromagnetic shower. The selection cuts are:

- ID = 10 or 11
- $|\text{detector } \eta| < 1.1$
- $p_T > 25$ GeV
- 7×7 H-matrix $\chi^2 > 20$

This rejects events with genuine electrons or photons and provides us with an estimate of the shape of the invariant mass spectrum of events with misidentified electrons and photons. In addition to the nominal selection above, we tried two different reverse 7×7 H-matrix χ^2 cuts.

- Set 1 : At least one electromagnetic object with 7×7 H-matrix $\chi^2 > 35$
- Set 2 : Both electromagnetic object with 7×7 H-matrix $\chi^2 > 20$

We found that the change in the total background prediction between these samples is negligibly small (Table III). Figure 1 shows the instrumental background distribution for the three different selections. Figure 2 shows the ratios of the instrumental background spectra.

Graviton Mass (GeV)	Mass Window (GeV)	background events		
		Set 1	Set 2	Nominal
200	190-210	82.2	88.1	83.8
300	280-320	26.6	26.0	26.9
400	380-420	5.9	5.8	5.9
500	450-550	5.5	5.4	5.3
600	550-650	1.9	1.9	1.8
700	620-780	0.8	0.9	0.8

TABLE III: Total number of predicted background events for different selections of instrumental background.

In order to determine the number of background events, we fit the invariant mass spectrum observed in collider data around the Z peak in the interval $60 < m(ee) < 140$ GeV with a superposition of the physics background shape and the instrumental background shape. Around the Z peak no new physics is expected. Therefore the total data should be well represented by a weighted sum of the total physics background and the instrumental background. We write the background spectrum as

$$h_{bkg} = f \times h_{inst} + (1 - f) \times h_{phys},$$

where h_{inst} and h_{phys} are the normalized invariant mass spectra from instrumental and physics background, respectively. The parameter f is varied to minimize the χ^2 between h_{bkg} and the invariant mass spectrum from the collider data, h_{data} . The minimization is done with root using TMinuit. The χ^2 is calculated as follows.

- number of data events in bin $i = n_i$
- total number of data events within the fit range = $N = \sum_i n_i$
- number of instrumental background events in bin $i = n'_i$

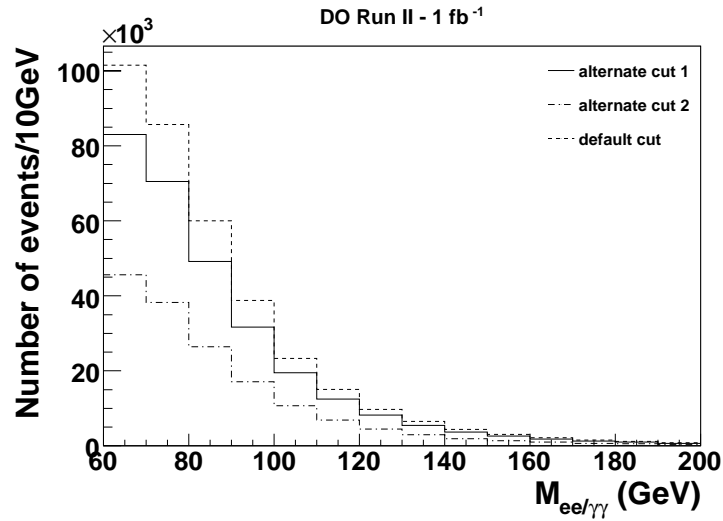


FIG. 1: Instrumental background distribution for the three different selections.

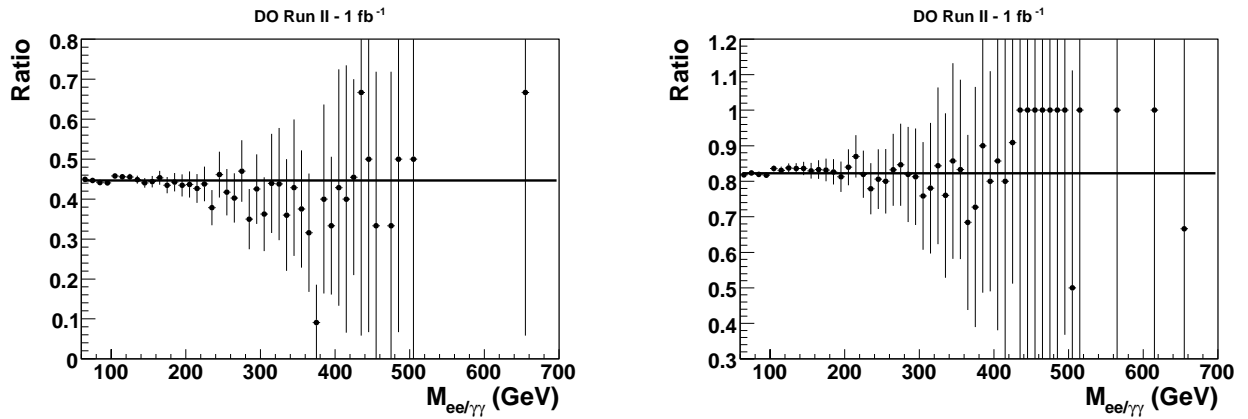


FIG. 2: Ratio of the instrumental background spectra for Set2/Set3 (left) and for Set1/Set3 (right).

- total number of instrumental background events within the fit range = $N' = \sum_i n'_i$
- contents of bin i of the normalized instrumental background spectrum = $a_i = n'_i/N'$
- number of physics background events in bin $i = n''_i$
- total number of physics background events within the fit range = $N'' = \sum_i n''_i$
- contents of bin i of the normalized physics background spectrum = $b_i = n''_i/N''$

$$\chi^2 = \sum_i \frac{(n_i - N(f \times a_i + (1-f) \times b_i))^2}{\delta^2}$$

where

$$\delta^2 = n_i + \left(\frac{Nf}{N'}\right)^2 n'_i + \left(\frac{N(1-f)}{N''}\right)^2 n''_i$$

Here, the sum is over the number of bins i within the fit range $60 \text{ GeV} < \text{mass} < 140 \text{ GeV}$. It is found that the best agreement is reached for $f = 0.199 \pm 0.0038$. Figure 3 shows the plot of χ^2 vs f . Figures 4 and 5 show the invariant mass spectra for data and the fitted background composition superimposed.

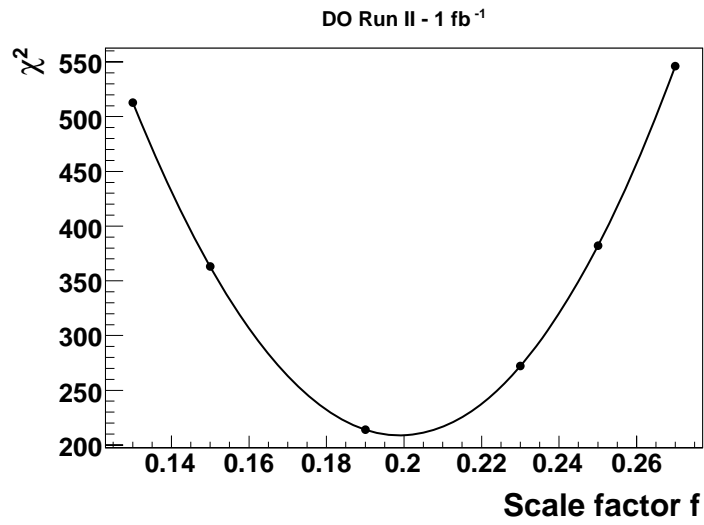


FIG. 3: χ^2 vs scale factor f for instrumental background.

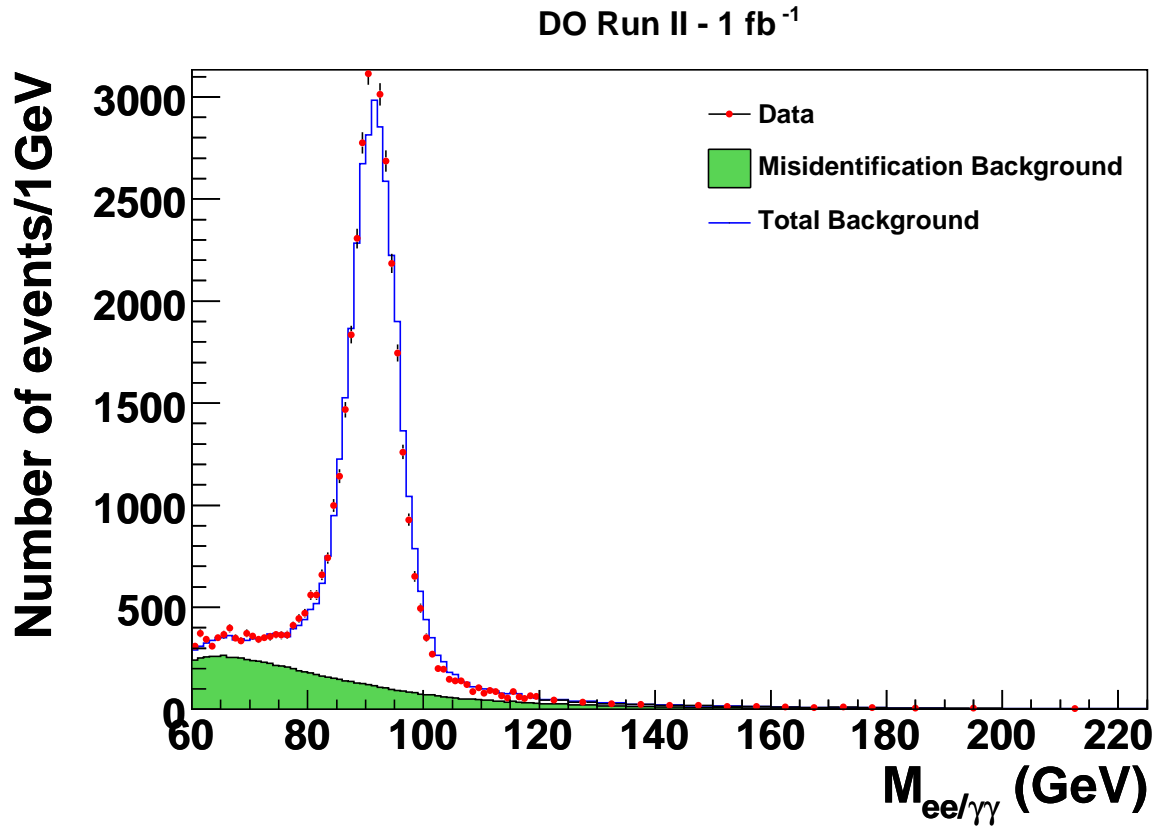


FIG. 4: Invariant mass spectrum from data (points) with the fitted total background shape (open histogram) and the fitted contribution from instrumental backgrounds (shaded histogram) superimposed.

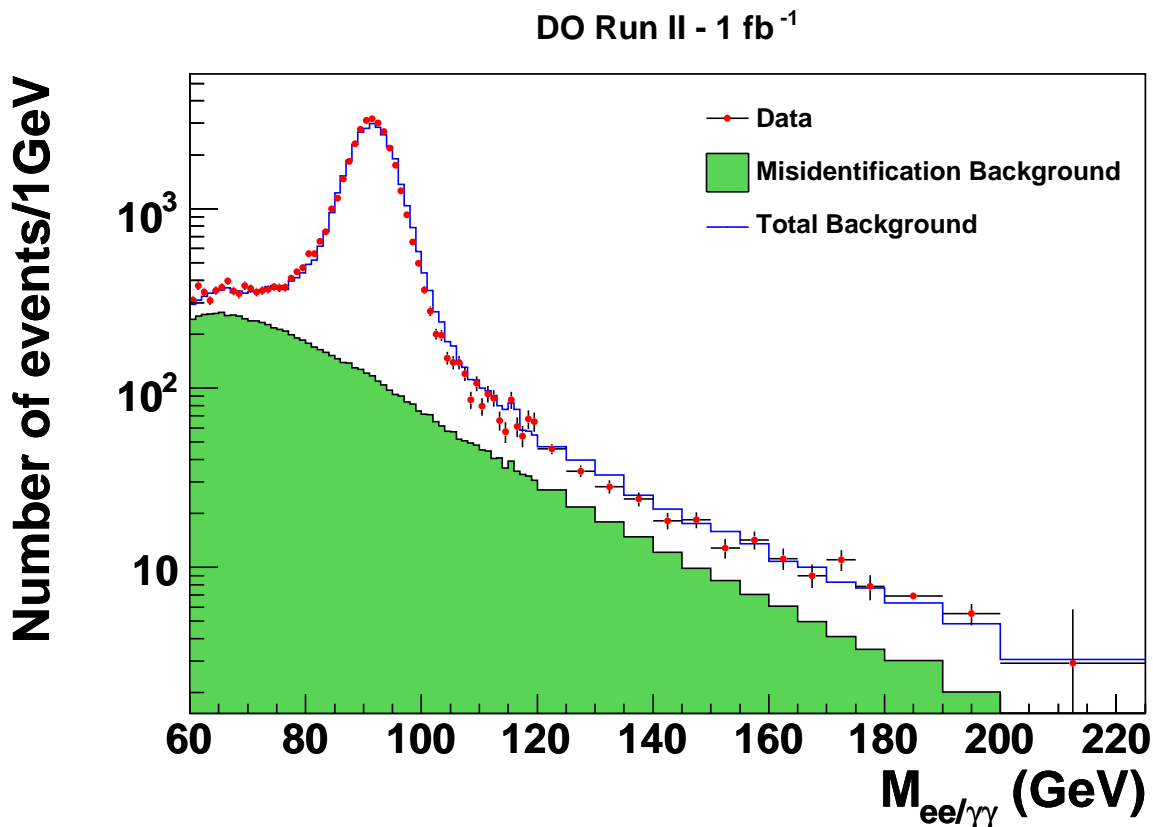


FIG. 5: Invariant mass spectrum from data (points) with the fitted total background shape (open histogram) and the fitted contribution from instrumental backgrounds (shaded histogram) superimposed.

Finally, having normalized the physics and instrumental background contributions, we can predict the shape of the invariant mass spectrum above 140 GeV and compare to collider data. This is done by applying the same scale factor $f = 0.199$ to the full invariant mass spectrum of instrumental background and a scale factor of $(1-f)$ to the full invariant mass spectrum of physics background. Adding these two weighted mass distribution gives the total background spectrum. Figure 6 shows the full mass spectra for data, the total background and the instrumental background contributions.

Table IV lists the number of events expected and observed above a number of invariant mass thresholds. The agreement between model prediction and observed number of events is very good except for $M > 100$ GeV. This arises from the slight resolution mismatch that we observe between data and Monte Carlo. To check whether this affects the results of our analysis we smeared the data with an additional constant term so that its resolution agrees with the MC. We cannot easily fix the MC because that would require undoing the smearing that was applied. We then repeat the background fit and find that $f = 0.199$ gives best agreement between data and MC. This change gives rise only to imperceptible differences in the model prediction ($\ll 1\%$). We further checked how much the data spectrum would change with the additional smearing at high mass and found that for thresholds of 300 GeV or more the expected number of events does not change by more than an event from the values in Table IV. We thus conclude that this resolution mismatch does not affect our background model prediction significantly.

M(GeV) >	60	100	140	150	200	250	300	350	400	450	500
Data	43639	3994	861	678	224	101	54	29	11	5	3
Total Background	43641	4513	863	667	221	95.7	44.7	23.5	13	7.5	4.5

TABLE IV: Number of data and background events above a mass threshold for the full mass spectra.

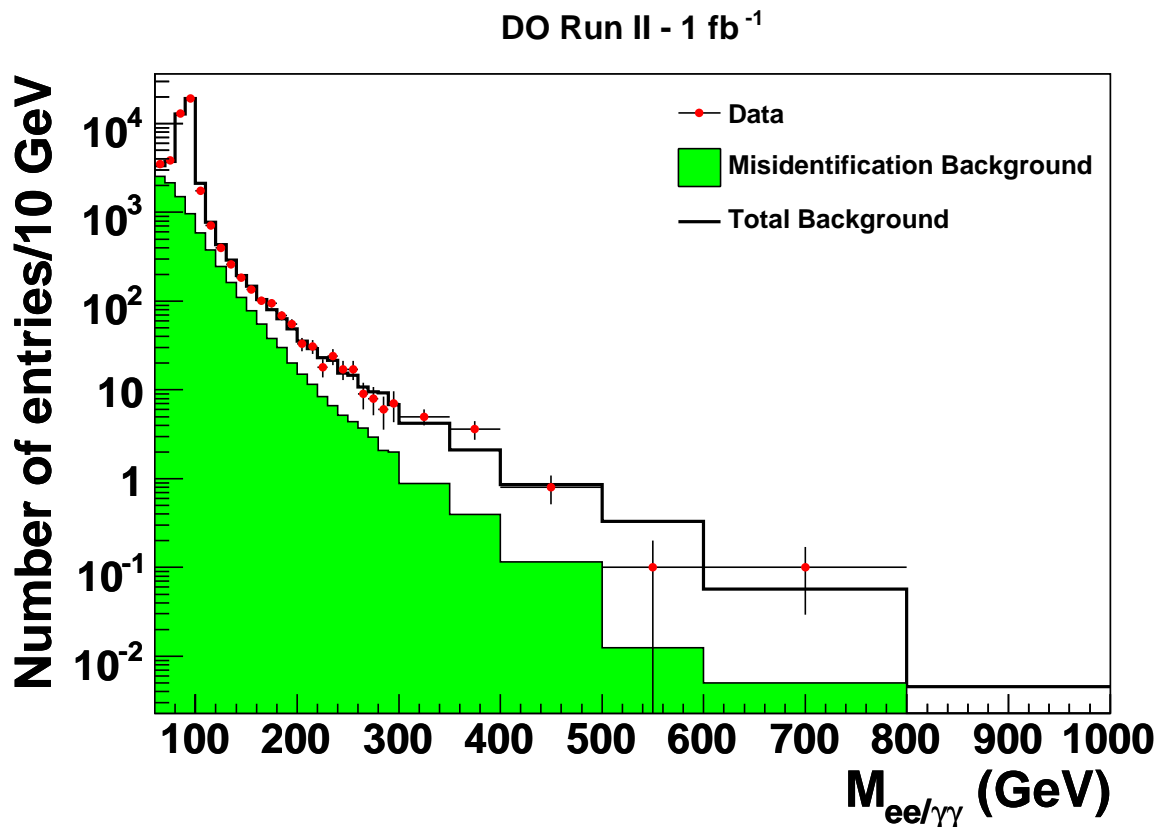


FIG. 6: Invariant mass spectrum from collider data (points) with expected total background (open line histogram) and instrumental background (shaded histogram) superimposed.

VI. LIMIT CALCULATION

The integrated luminosity of our data sample is extracted from the scale factor for the DY spectrum determined in section V. We take the LO cross section listed in Table I and assume a mass independent k-factor of 1.34[8] to get the next to leading order (NLO) cross-section. The integrated luminosity is calculated using the following steps:

- Number of generated Drell-Yan MC events (Sample generated with invariant mass between 60 and 130 GeV) : N_{DY}
- Number of generated Diphoton MC events (Sample generated with invariant mass between 50 and 130 GeV): $N_{\gamma\gamma}$
- Drell-Yan NLO cross-section : σ_{NLO}^{DY}
- Diphoton NLO cross-section : $\sigma_{NLO}^{\gamma\gamma}$
- Number of data events with invariant mass between 60 GeV and 140 GeV : A
- Number of Drell-Yan Monte Carlo events with invariant mass between 60 GeV and 140 GeV : B
- Number of diphoton Monte Carlo events with invariant mass between 60 GeV and 140 GeV : C
- The total number of Drell-Yan and diphoton events in data is $N = A \times (1 - f)$ where f is the scale factor from section V.
- The total number of standard model background (Drell-Yan + diphoton) should be equal to N given by

$$N = \mathcal{L} \times \frac{1}{r^2} \left(\sigma_{NLO}^{DY} \times \frac{B}{N_{DY}} + \sigma_{NLO}^{\gamma\gamma} \times \frac{C}{N_{\gamma\gamma}} \right),$$

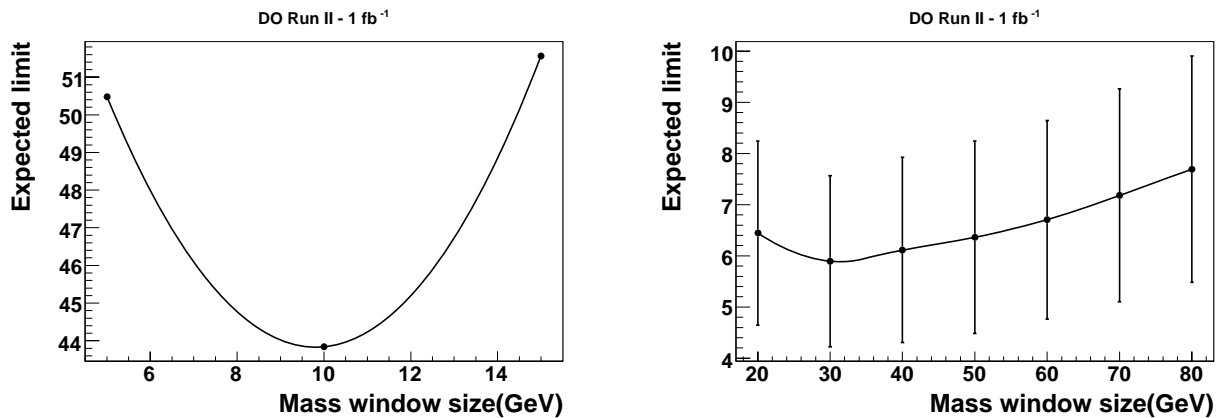


FIG. 7: Expected limit as a function of the width of the mass window for $M_1 = 200$ GeV (left) and $M_1 = 500$ GeV (right).

where r is the data/MC scale factor for the efficiencies.

The integrated luminosity (\mathcal{L}) is calculated solving this equation for \mathcal{L} . The calculated integrated luminosity with the numbers listed in Table V is $0.985 \pm 0.035 \text{ fb}^{-1}$. This is about 1.1 standard deviations lower than the value we obtain from the D0 luminosity database ($1.068 \pm 0.065 \text{ fb}^{-1}$).

N_{DY}	σ_{NLO}^{DY} (pb)	B	$N_{\gamma\gamma}$	C	$\sigma_{NLO}^{\gamma\gamma}$ (pb)	A	f	r
264750	178×1.34	40732	50500	923	42.7×1.34	42778	0.199	0.96

TABLE V: Values for integrated luminosity calculation.

The signal acceptance is obtained from RS graviton MC. For a given graviton mass, the acceptance is defined by:

$$\epsilon_{total} = \frac{N_{pass}}{N_{total}}$$

N_{total} is the total number of MC events generated for a given graviton mass, and N_{pass} is the number of MC events that pass all the selection cuts and mass window cuts. This efficiency is further corrected to account for the difference between data and Monte Carlo by a correction factor $r = 0.96$ (detail in section VII C). The mass window cuts applied for the different mass points are listed in the Table VI. These mass windows are optimized based on the prescription described in [9]. In the first step, the invariant mass spectrum for each graviton mass sample is fitted with a gaussian and from that fit the width σ is obtained. Then the optimum mass window, following the prescription [9] is $2 \times \sigma$. If the expected number of background events is less than 1, the mass window used is $3 \times \sigma$. The window size has been rounded to match the histogram bin size of 10 GeV. As a cross check, we also carried out a separate study varying the width of the mass windows and calculating the corresponding expected limit. Figure 7 shows the expected limit as a function of the width of the mass window for $M_1 = 200$ GeV and 500 GeV.

The number of data and expected background events were calculated by integrating the invariant mass spectra (Fig. 6) for data and total background over different mass windows corresponding to each graviton mass. The results are listed in Table VI. The systematic uncertainties used for the limit calculation are listed in Table VII and the details are discussed in section VII.

The Bayesian Limit calculator [10] was used to calculate the lower limit on the cross section \times branching fraction at 95% confidence level. The inputs for the Bayesian limit calculator for a given graviton mass are:

- Number of observed event within the mass window : N
- Number of expected (background) event within the mass window : b
- The signal acceptance : ϵ
- Integrated luminosity : \mathcal{L}
- Systematic uncertainties on b and ϵ

With these inputs, the limit calculator calculates the observed 95% confidence level upper limit. The expected limit for a given graviton mass is calculated by equating the number of observed events with the number of background events (i.e. $N = b$). For graviton mass for which the predicted number of background event is less than 5, we compute the poisson averaged expected limit

$$\langle \sigma_{95} \rangle = \frac{\sum_{n=n_{min}}^{n=n_{max}} P_n \times \sigma_{95}^n}{\sum_{n=n_{min}}^{n=n_{max}} P_n}$$

Here P_n is the poisson probability to observe n events when b events are expected, $n_{min} = b - 2\sqrt{b}$, $n_{max} = b + 2\sqrt{b}$, and σ_{95}^n is the 95% confidence level upper limit on the cross section obtained for n observed events.

Since we accept e^+e^- and $\gamma\gamma$ final states we obtain a limit on the sum of these two decay channels. The branching fraction to $\gamma\gamma$ is twice that to e^+e^- . We quote a limit on $\sigma(\bar{p} \rightarrow G + X) \times B(G \rightarrow e^+e^-)$ which is therefore a third of the limit on $\sigma(\bar{p} \rightarrow G + X) \times [B(G \rightarrow e^+e^-) + B(G \rightarrow \gamma\gamma)]$.

The results of the limit calculation are listed in Table VI. Figure 8 shows the 95% confidence level upper limit on $\sigma(\bar{p} \rightarrow G + X) \times B(G \rightarrow e^+e^-)$ versus the graviton mass compared to the theoretical prediction. Here we use the LO cross section obtained with PYTHIA[6], multiplied by a mass independent k-factor of 1.34[8]. Based on data from 0.985 fb^{-1} , we can thus exclude masses for the RS graviton upto 898(303) GeV at 95% confidence level for $\kappa/\overline{M}_{Pl} = 0.1(0.01)$. The published limit based on 275 pb^{-1} was 785(250) GeV for $\kappa/\overline{M}_{Pl} = 0.1(0.01)$. Figure 9 shows the upper limit on the coupling parameter κ/\overline{M}_{Pl} as a function of graviton mass M_1 . The total cross-section (graviton production cross-section \times branching fraction) is proportional to the square of the coupling, ($\sigma \sim (\kappa/\overline{M}_{Pl})^2$). Using this relation, the following equation is obtained:

$$\frac{(\kappa/\overline{M}_{Pl})_{95\%CL}}{0.1} = \sqrt{\frac{\sigma_{95\%CL}}{\sigma_{0.1}}}$$

With $\sigma_{0.1}$, the theoretical cross-section (graviton production cross-section \times branching fraction) for coupling 0.1 and $\sigma_{95\%CL}$, the calculated 95% confidence level upper limit on the total cross-section, the 95% confidence level upper limit on coupling, $(\kappa/\overline{M}_{Pl})_{95\%CL}$, is calculated.

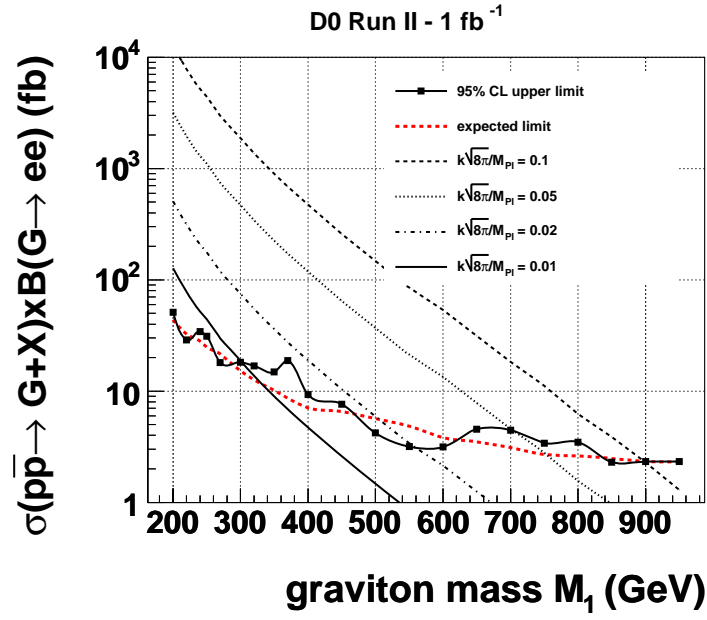


FIG. 8: 95% confidence level upper limit on $\sigma(\bar{p} \rightarrow G + X) \times B(G \rightarrow e^+e^-)$ from 1 fb^{-1} of data compared with the sensitivity and the theoretical predictions for different couplings κ/\overline{M}_{Pl} .

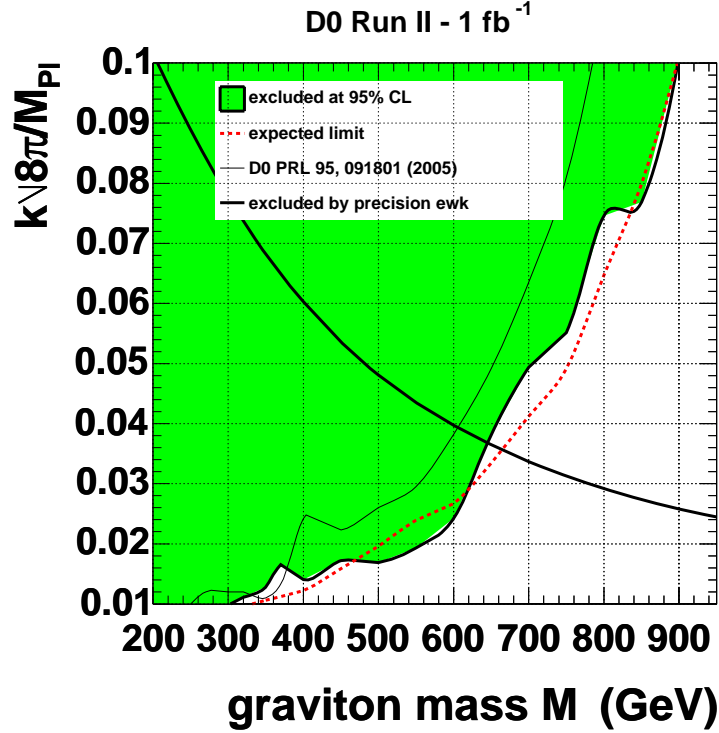


FIG. 9: 95% confidence level upper limit on κ/\overline{M}_{Pl} versus graviton mass M_1 from 1 fb^{-1} of data compared with the expected limit and the previously published exclusion contour[4].

Mass (GeV)	Mass Window (GeV)	Data	Total Background	ϵ_{Total} for signal	Cross Section (fb)			Coupling	
					theory	expected limit	observed limit	expected limit	observed limit
200	190-210	88	83.8±7.3	0.208±0.030	12730	43.9	51.0	0.0058	0.0063
220	210-230	49	52.4±4.7	0.214±0.033	7861	32.5	28.7	0.0064	0.0060
240	230-250	41	37.1±3.7	0.211±0.038	5181	28.1	34.3	0.0073	0.0081
250	240-260	34	30.1±3.1	0.215±0.038	4417	24.7	31.0	0.0074	0.0083
270	250-290	40	44.0±4.5	0.297±0.026	2988	21.6	18.0	0.0085	0.0077
300	280-320	29	26.9±3.0	0.310±0.029	1885	15.2	18.2	0.0089	0.0098
320	300-340	22	18.3±2.0	0.318±0.036	1371	12.6	16.9	0.0095	0.0110
350	330-370	15	11.4±1.2	0.311±0.034	902	10.2	14.8	0.0106	0.0128
370	350-390	16	8.8±0.96	0.316±0.039	688	8.6	18.8	0.0111	0.0165
400	380-420	7	5.9±0.69	0.319±0.042	473	7.0	9.3	0.0122	0.0140
450	420-480	6	4.9±0.58	0.366±0.021	259	6.5	7.6	0.0158	0.0171
500	450-550	3	5.3±1.01	0.419±0.014	147	5.6	4.2	0.0196	0.0168
550	500-600	1	3.3±0.89	0.434±0.015	84.9	4.8	3.1	0.0238	0.0193
600	540-660	1	1.84±0.22	0.454±0.017	53.6	3.8	3.1	0.0266	0.0242
650	590-710	2	1.04±0.13	0.437±0.013	31.3	3.4	4.5	0.0334	0.0381
700	620-780	2	0.84±0.10	0.458±0.013	18.3	3.1	4.4	0.0412	0.0493
750	660-840	1	0.51±0.06	0.473±0.015	11.2	2.7	3.4	0.0491	0.0551
800	700-900	1	0.32±0.04	0.474±0.015	6.2	2.6	3.4	0.0647	0.0746
850	750-950	0	0.18±0.02	0.481±0.013	3.9	2.4	2.2	0.0799	0.0768
900	790-1010	0	0.108±0.02	0.475±0.014	2.3	2.3	2.3	0.1010	0.1010
950	840-1060	0	0.059±0.01	0.474±0.012	1.3	2.3	2.3	0.1340	0.1340

TABLE VI: Number of expected and observed events in different mass windows, signal acceptance and upper limit on cross section \times branching ratio.

VII. SYSTEMATIC UNCERTAINTIES

The different sources of uncertainties as listed in Table VII and how they were calculated, are described here in detail.

Source of Signal Uncertainty	Uncertainty
pdf uncertainty	0.2% – 5.5%
Resolution	1% – 11.1%
EM ID uncertainty	1.4%
Statistical uncertainty	0.5%
Total	2% – 12.4%
Source of Background Uncertainty	Uncertainty
k-factor mass dependence	5.2%
Uncertainty on f due to trigger	6%
Statistical uncertainty	2% - 24%
Uncertainty on relative cross-section due to pdf	2% - 10%
Total	8.4%-27%

TABLE VII: Sources of uncertainty for signal and background.

A. Uncertainty due to trigger efficiency

From previous studies [11] it is known that the EM triggers are almost 100% efficient at high mass. In the previous RS Graviton search [4] at $D\bar{O}$ it was taken to be fully efficient mainly because this analysis is only concerned with high P_T EM objects. In the following, we estimate the effect of the trigger thresholds and show that it is small.

- The eight triggers, their corresponding trigger versions and the integrated luminosity corresponding to each of these triggers, are listed in Table VIII.

Trigger	Trigger name	Trigger version	Integrated luminosity pb ⁻¹
Single-EM	EM_MX_SH	V8 to V11	122
	E1_SH30	V12 and V13	596
	E1_SHT22	V13	377
	E1_SH35	V14	350
Di-EM	2EM_HI	V8 to V11	122
	E1_2L15_SH15	V12 and V13	596
	E1_2L20	V12 and V13	596
	E1_2L20_L25	V14	350

TABLE VIII: List of triggers that pass 97% of the skimmed data.

- The trigger efficiency as a function of transverse momentum (p_T), were obtained from an independent trigger efficiency study done at $D\bar{O}$ [12]. Figure 10 shows the turn-on curves for the four single electron triggers used for this study.
- For a given single electron trigger, the total efficiency was calculated using the following equation:

$$\epsilon_{Total} = \epsilon_1 \times (1 - \epsilon_2) + \epsilon_2 \times (1 - \epsilon_1) + \epsilon_1 \times \epsilon_2$$

Here, ϵ_1 and ϵ_2 are the trigger efficiencies for the two electromagnetic objects in a selected event. The total efficiency for a given event is the probability that one or both electromagnetic objects will pass the trigger.

- Calculate the integrated luminosity weighted average for the four trigger versions using the equation :

$$\mathcal{W}_{Total} = \frac{\epsilon_{Total}^{EM-MX-SH} \times 122 \text{ pb}^{-1} + \epsilon_{Total}^{E1-SH30} \times 219 \text{ pb}^{-1} + \epsilon_{Total}^{E1-SHT22} \times 377 \text{ pb}^{-1} + \epsilon_{Total}^{E1-SH35} \times 350 \text{ pb}^{-1}}{1068 \text{ pb}^{-1}}$$

This gave the total probability (weight) that the selected event will pass a logical OR of these four single EM triggers.

- The total background invariant mass spectrum is obtained with unweighted MC as described in section V.
- Next, the Drell-Yan and Diphoton Monte Carlo invariant mass spectra are obtained applying the weights calculated (\mathcal{W}_{Total}) and then the total background invariant mass spectrum is obtained using these weighted MC.
- Compare the two distributions.

Figure 11 shows the plot comparing the mass spectra of the total background with weighted and unweighted Monte Carlo. The effect of the trigger was checked in the low mass region, which is used to fit the QCD background to calculate the integrated luminosity as described in section VI. The difference in the integrated luminosity calculated using weighted Monte Carlo and unweighted Monte Carlo came out to be less than 1% (Table IX). Also, the change in total predicted background with and without the trigger turnons is only a few percent as shown in Table X

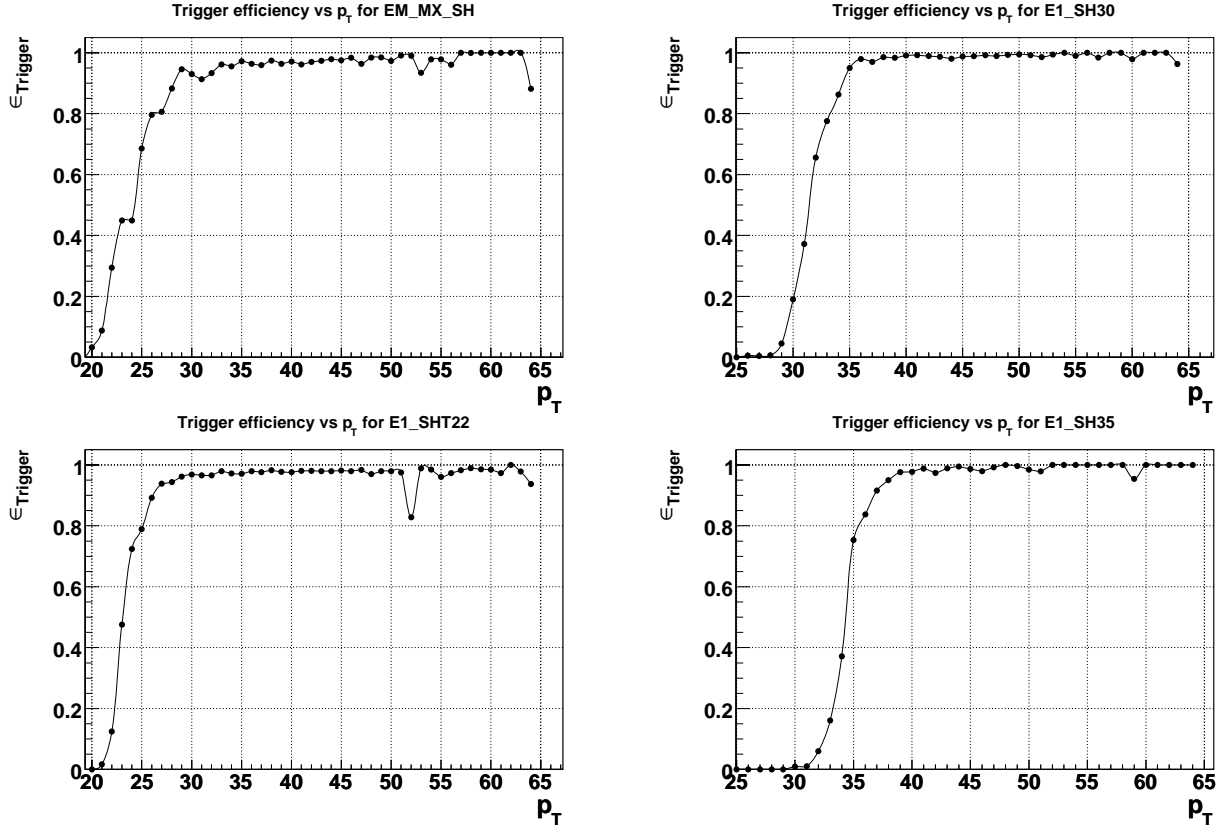


FIG. 10: Trigger turn-on curves for EM_MX_SH (top left), E1_SH30 (top right), E1_SHT22 (bottom left), and E1_SH35 (bottom right)[12]

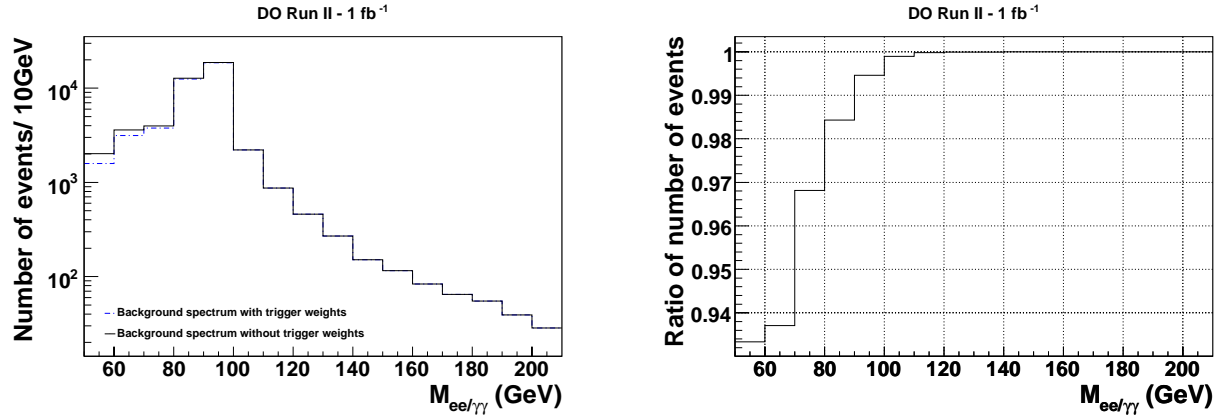


FIG. 11: Comparison of the mass spectra for total background with trigger weights and without trigger weights. At higher masses the spectra are identical.

	with trigger turnon	without trigger turnon	change (%)
f	0.211	0.199	6
Integrated luminosity	987 pb ⁻¹	985 pb ⁻¹	0.2

TABLE IX: Change in f and in integrated luminosity with and without trigger turnons.

Graviton Mass (GeV)	Total background (with trigger turnon)	Total background (without trigger turnon)	$\Delta b/b$ %
200	86.2	83.8	2.8
300	27.4	26.9	1.8
400	5.97	5.89	1.3
500	5.38	5.33	0.9
600	1.85	1.84	0.5
700	0.84	0.84	0.0

TABLE X: Change in total background (b) with and without trigger turnons.

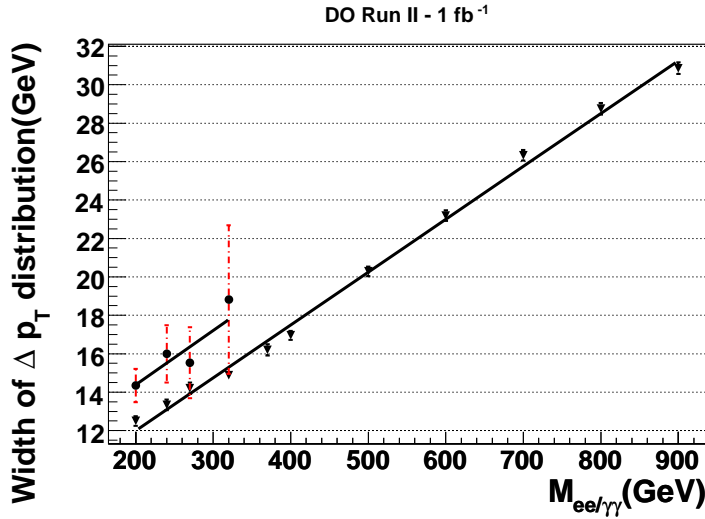
B. Uncertainty due to resolution

To calculate the signal efficiency, a mass window cut is applied. The uncertainty in the acceptance of the mass window due to the energy resolution is estimated. First the Δp_T distribution for the two electromagnetic objects is obtained. The Δp_T is the difference in the transverse momentum (p_T) between the two EM objects in a selected event. The idea behind this is, the two electromagnetic objects selected after the selection cuts are expected to be back to back with Δp_T around zero. In order to reduce the background in the Δp_T distribution, we require $|\Delta\phi| > 2.6$ in addition to the selection cuts. After that, the distribution is fitted with a gaussian and the width is obtained. This is done for several mass points. Figure 12 plots σ vs mass for data and MC. The data and MC distributions are then fitted with first order polynomial. The parameters for the fits obtained for data and MC are listed in Table XI.

Next the ratio of the width for data and MC is obtained using the equation:

$$R = \frac{8.72 + \text{mass in GeV} \times 0.02}{6.48 + \text{mass in GeV} \times 0.02}$$

Next, the mass window applied to get the signal efficiency for a given graviton mass is reduced by the corresponding

FIG. 12: Width of the Δp_T distribution for data(circle) and MC(triangle).

Sample	par[0]	par[1]
Data	8.72	0.02
MC	6.48	0.02

TABLE XI: Parameters for the fit from figure 12.

factor R obtained and the signal efficiency for the reduced mass window is obtained. The fractional uncertainty is calculated as $\Delta\epsilon/\epsilon$, where $\Delta\epsilon$ is the change in efficiency when the width of the mass window is changed.

The values for R and $\Delta\epsilon/\epsilon$ for the different graviton masses are listed in Table XII. For each graviton mass value the uncertainty from this table is used in the limit setting procedure.

Graviton Mass (GeV)	R	$\Delta\epsilon/\epsilon$ %
200	1.20	9.6
220	1.19	9.8
240	1.19	10.9
250	1.18	11.1
270	1.18	4.7
300	1.17	5.1
320	1.16	5.6
350	1.16	6.4
370	1.15	6.3
400	1.15	6.8
450	1.14	4.6
500	1.13	1.4
550	1.13	2.3
600	1.12	1.5
650	1.12	1.6
700	1.11	1.1
750	1.11	1.3
800	1.10	1.1
850	1.10	1.0
900	1.10	1.3
950	1.09	0.8

TABLE XII: Uncertainty on signal efficiency due to resolution.

C. EM ID uncertainty

This uncertainty originates from the difference in electron/photon identification efficiency between data and MC. The preselection efficiency is 100% both in data and in MC[7]. The tag and probe method is used to get the ID efficiency for data. First events with two electromagnetic objects are selected. Then we require that the tag object passes all the cuts which are defined in section IV. In addition to these cuts, the tag object is also required to have a track match. The other object we probe, passed the following set of cuts:

- Loose cut for probe object
 - ID = 10 or 11
 - $|\text{detector } \eta| < 1.1$
 - $p_T > 25 \text{ GeV}$

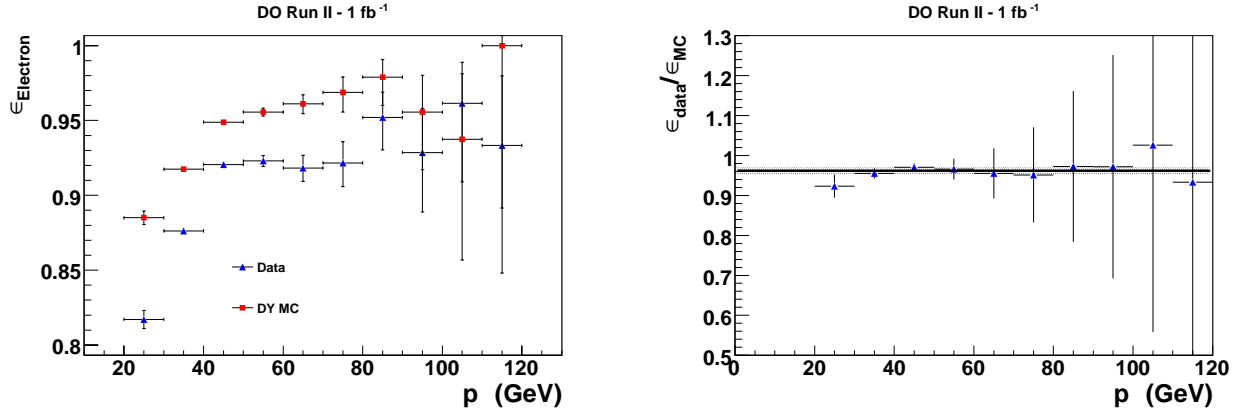


FIG. 13: Comparison of electron efficiencies vs p_T for MC and data in CC. The right plot shows the ratio of data and MC efficiencies as a function of p_T . The line is a fit to a constant.

- fraction of energy in electromagnetic calorimeter $f_{EM} > 0.9$
- fraction of energy in isolation cone $f_{iso} < 0.2$

Counting the number of events with $85 < m(ee) < 100$ GeV gives the number of Z events with loose cuts on the probe electron N_{loose} . Next, all the selection cuts for electromagnetic showers defined in section IV are applied on the probe electron to determine the number of Z events with selection cuts on the probe electron N_{sel} in exactly the same way. The electron ID efficiency is then given by

$$\epsilon_{ID} = \frac{N_{sel}}{N_{loose}}.$$

Exactly the same procedure is followed to get the efficiency for Drell-Yan MC sample. Then the electron ID efficiency is plotted as a function of p_T for both Data and MC (Figure 13). This shows the difference in the EM ID efficiency between data and MC. We fit the ratio of the EM ID efficiency for Data and MC to a constant. The value obtained from this fit is $r = 0.961 \pm 0.007$. The event efficiency has to be corrected by r^2 because every event contains two electromagnetic objects. Thus we quote a total EM object uncertainty of 1.4%.

D. Statistical uncertainties in MC and control data samples

The statistical uncertainty in the signal efficiency ϵ_{total} is given by the standard binomial uncertainty

$$\frac{\sqrt{N_{total} \times \epsilon_{total} \times (1 - \epsilon_{total})}}{N_{total}},$$

where N_{total} is the total number of signal Monte Carlo events for a given graviton mass (section VI). This uncertainty is small (about 0.5%) and can be neglected.

The statistical uncertainty on the number of predicted background events is obtained for each mass window by propagating the statistical uncertainties in the DY, $\gamma\gamma$, and instrumental background distributions. The results for the different mass points are listed in Table XIII.

E. Mass dependence of k-factor

To get the NLO cross-section, a mass independent k-factor of 1.34[8] is used. However, the k-factor is not exactly mass independent and hence, it is a source of uncertainty. Figure 14 shows the mass dependence of k-factor[13]. With an uncertainty band of ± 0.07 around 1.34, the uncertainty on the k-factor due to mass dependence is 5.2%.

Graviton Mass (GeV)	Total background	Statistical uncertainty on total background	Relative uncertainty %
200	83.84	2.12	2.53
220	52.38	1.76	3.37
240	37.12	1.72	4.64
250	30.13	1.54	5.13
270	44.03	1.97	4.48
300	26.94	1.65	6.15
320	18.32	0.96	5.25
350	11.40	0.41	3.59
370	8.76	0.36	4.11
400	5.89	0.28	4.91
450	4.89	0.26	5.50
500	5.33	0.84	15.7
550	3.31	0.82	24.7
600	1.84	0.069	3.78
650	1.04	0.056	5.39
700	0.84	0.049	5.86
750	0.51	0.019	3.80
800	0.32	0.015	4.75
850	0.18	0.011	6.45
900	0.108	0.0088	8.18
950	0.059	0.0065	10.9

TABLE XIII: Background statistical uncertainty.

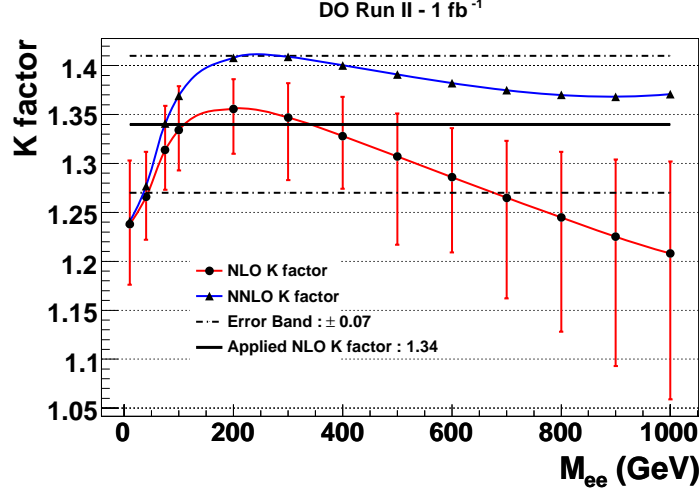


FIG. 14: Mass dependence of k-factor[13].

F. Proton structure uncertainty

The parton distribution function (pdf) uncertainty is calculated by using the pdf reweight procedure as described in Ref.[14]. For the CTEQ6.1M pdf set[15], a central pdf set and 2×20 sets of error pdfs are provided. The advantage of this method is, generating MC samples for the different pdfs is not required. Instead, for each error pdf, a weight is applied. The CAF processor `caf_pdfreweight`[16], is used for this study which provides the weight. The general

method of calculating the pdf uncertainty for a given observable is explained below. For this analysis, the observables are efficiency and cross-section.

- The value of a given observable is obtained for the LO pdf (CTEQ6L1)[17] - A .
- The value of the observable for the NLO (CTEQ6.1M) central pdf is obtained - B .
- The value of the observable for the $i=1-40$ (2×20) error pdfs is obtained - B_i
- The deviation is calculated - $B - B_i$
- the positive uncertainty δ_{pdf}^+ is the sum in quadrature of all positive deviations $(B - B_i) > 0$ scaled to the value of the LO observable:

$$\delta_{pdf}^+ = \frac{A}{B} \times \sqrt{\sum_i (B - B_i)^2},$$

where the sum runs only over the positive deviations.

- the negative uncertainty δ_{pdf}^- is calculated similarly, except that the sum now runs only over the negative deviations.

The final result is quoted as $A + \delta_{pdf}^+ - \delta_{pdf}^-$. In this analysis, following the method described above, the pdf uncertainty was calculated for the signal efficiency and the direct diphoton and Drell-Yan cross-section.

RS Graviton Mass (GeV)	Positive uncertainty %	Negative uncertainty %
200	4.6	5.2
220	4.7	5.1
240	4.6	5.2
250	3.7	4.4
270	4.5	5.5
300	3.1	3.9
320	4.2	5.3
350	2.9	3.7
370	3.4	4.4
400	3.4	4.4
450	2.8	3.9
500	1.6	2.3
550	1.5	2.0
600	1.7	2.7
650	1.3	2.1
700	1.1	1.8
750	1.1	2.1
800	1.0	2.1
850	0.5	1.1
900	0.7	1.8
950	0.2	0.2

TABLE XIV: Uncertainty (positive and negative) of signal efficiency due to pdf for different graviton mass.

1. *Signal efficiency uncertainty due to pdf*

To define the efficiency ϵ_{pdf} for a given error pdf we define the subset \mathbf{X} of all event indices $i \in [1, \dots, N]$ for which the event passes the selection cuts. Then

$$\epsilon_{pdf} = \frac{\sum_{i \in \mathbf{X}} W_i^{pdf}}{\sum_{i=1}^N W_i^{pdf}}.$$

Here W_i^{pdf} is the weight of event i for a given error pdf. The signal efficiency uncertainty due to pdf for different graviton mass is listed in Table XIV. For limit calculation, a mass dependent uncertainty on efficiency due to pdf, is used and for each graviton mass, the larger of the two uncertainties (positive or negative) is taken.

2. *Uncertainty on cross-section due to pdf*

The cross-section was obtained from the mean value of the root tuple for each MC sample. The cross section for the physics background of Drell-Yan and diphoton production for a given error pdf is given by:

$$\sigma_{pdf} = \sigma^0 \frac{\sum_{i=1}^N W_i^{pdf}}{\sum_{i=1}^N W_i^0}$$

Here W_i^0 is the weight of event i and σ^0 is the cross section for the reference pdf. The sum i runs over the N events in the MC sample. Finally the central value and the positive and negative uncertainty on the cross-section ($\sigma + \delta^+ - \delta^-$) is obtained for each of the Drell-Yan and diphoton MC samples. The central value and their corresponding uncertainties for the different MC samples are listed in Table XV.

MC Sample	MassWindow (GeV)	Cross-Section(NLO) (pb)	δ^+ (pb)	δ^- (pb)
DY	60-130	238.5	8.0	8.7
	130-250	1.74	0.060	0.064
	250-500	0.14	0.0064	0.0065
	>500	0.0060	0.00034	0.00043
$\gamma\gamma$	50-130	57.2	2.19	2.64
	130-250	4.1	0.18	0.20
	250-500	0.65	0.031	0.031
	>500	0.455	0.026	0.032

TABLE XV: NLO cross-section with uncertainty (due to PDF) for the DY and $\gamma\gamma$ MC samples.

Mass Window (GeV)	$\frac{\sigma_{DY}}{\sigma_{\gamma\gamma}}$	$\frac{\sigma_{DY}^+}{\sigma_{\gamma\gamma}^+}$	$\frac{\sigma_{DY}^-}{\sigma_{\gamma\gamma}^-}$	Uncertainty (%)
60-130	4.16	4.51	3.86	15.6
130-250	0.42	0.45	0.39	14.2
250-500	0.21	0.24	0.20	19.0
>500	0.013	0.014	0.011	22

TABLE XVI: Ratio of DY and diphoton cross-section.

For this analysis, the uncertainty comes from the relative normalization of the cross-sections for the DY and diphoton samples which may vary with pdf choice. The ratio of the cross-sections for the different samples are calculated for four different combinations and then the relative uncertainty is calculated. The numbers are summarized in Table XVI.

Graviton Mass (GeV)	Total background (K=1.34)	Total background (K=1.61)	Total background (K=1.07)	$\Delta b/b$ %
200	83.8	86.2	81.39	2.9
300	26.9	28.3	25.5	5.2
400	5.89	6.31	5.47	7.1
500	5.33	5.68	4.98	6.5
600	1.84	2.00	1.68	8.6
700	0.84	0.90	0.77	7.1
800	0.32	0.35	0.29	9.3
900	0.108	0.117	0.098	8.3

TABLE XVII: Change in total number of predicted background events for different k-factor for diphoton.

In this table we define $\sigma_{DY} + \delta_{DY}^+ = \sigma_{DY}^+$, $\sigma_{DY} - \delta_{DY}^- = \sigma_{DY}^-$, $\sigma_{\gamma\gamma} + \delta_{\gamma\gamma}^+ = \sigma_{\gamma\gamma}^+$ and $\sigma_{\gamma\gamma} - \delta_{\gamma\gamma}^- = \sigma_{\gamma\gamma}^-$. We make the conservative assumption that the two cross sections vary in a completely anticorrelated way with the pdfs. To estimate the effect of this variation, the k-factor for diphoton prediction is varied by $\pm 20\%$ from the actual value used (K=1.34) and the corresponding change in the total number of predicted background events is calculated. The relative change in the total background for the different k-factor is used as an uncertainty (Table XVII).

VIII. CONCLUSION

Using about 1 fb^{-1} of data from $p\bar{p}$ -collisions at $\sqrt{s} = 1.96 \text{ TeV}$, collected by the D0 detector at the Fermilab Tevatron between October 2002 and February 2006, we have searched for a narrow resonance in the invariant mass spectrum of two electromagnetic showers from electron-positron or photon pairs. The observed spectrum is in good agreement with predictions based on standard-model processes. In the framework of the Randall-Sundrum model with a warped extra dimension we set 95% confidence level upper limits on the production cross section times branching fraction into electron-positron pairs of the lightest Kaluza-Klein mode of the graviton between 51 fb and 2.3 fb for masses of 200 GeV and over 900 GeV, respectively. These translate into lower limits on the mass M_1 of the lightest Kaluza-Klein mode of the graviton of 303 GeV to 898 GeV for couplings of the graviton to standard model fields $\kappa/\overline{M}_{Pl} = 0.01$ to 0.1.

Acknowledgements

We would like to thank everyone who helped us at different stages of this analysis. We would especially like to thank Prof. Greg Landsberg, Dr. Arnd Meyer, Ioannis Katsanos, Subhendu Chakraborty and Junjie Zhu for their help and support.

-
- [1] L. Randall and R. Sundrum, Phys. Rev. Lett. 83, 3370 (1999); *ibid.*,83,4690 (1999).
 - [2] H. Davoudiasl, J.L. Hewett and T.G. Rizzo, Phys. Rev. Lett. 84, 2080 (1999)
 - [3] H. Davoudiasl, J.L. Hewett and T.G. Rizzo, Phys.Rev. D63 (2001) 075004
 - [4] D0 Collaboration, V.M.Abazov *et al.*, Phys. Rev. Lett. 95, 091801 (2005).
 - [5] CDF Collaboration, "The search for new physics in high-mass dielectron events in $p\bar{p}$ collisions at $\sqrt{s} = 1.96 \text{ TeV}$ ", CDF note 8694 (2007).
 - [6] T. Sjöstrand, L. Lönnbald, Pythia 6.2, hep-ph/0108264,2001.
 - [7] J.Hays, J.Mitrevski, C.Schwanenberger, T.Toole, "Single Electron Efficiencies in p17 Data and Monte-Carlo", D0 note 5025, April 2006.
 - [8] P.Mathews, V. Ravindran, K. Sridhar, and W.L. van Neerven, Nucl. Phys. B713, 333(2005).
 - [9] Greg Landsberg and Konstantin T.Matchev, Discovering a Light Higgs Boson with Light, Fermilab-Pub-00/003-T, hep-ex/0001007.
 - [10] I. Bertram *et al.*, A Recipe for the Construction of Confidence Limits, DØ Note 3476 (1998)

- [11] H. Kim and J. Yu, A Search for Wbb and WH Production in pp Collisions at $\sqrt{s} = 1.96$ TeV with Full Data Set of Pass2, DØ note 4706 (2006)
- [12] J. Hays *et al.*, Electron Trigger Efficiencies using Calorimeter Information in p17 Data, DØ note 5138 (2006)
- [13] R. Hamberg, W. L. van Neerven, T. Matsuura, A complete calculation of the order α_s^2 correction to the Drell-Yan K-factor, Nucl. Phys. B359, 343-405 (1991)
- [14] Volker Buescher *et al.*, Conclusions of Mini-Workshop on PDF uncertainties and related topics, DØ note 4618 (2004)
- [15] Daniel Stump, Joey Huston, Jon Pumplin, Wu-Ki Tung, H. L. Lai, Steve Kuhlmann and J. F. Owens, JHEP 0310 (2003) 046
- [16] Patrice Verdier and Kristian Harder, PDF reweighting processor for CAF (2006)
`file:///d0dist/dist/packages/caf_pdfreweight/devel/doc/index.html`
- [17] J. Pumplin, D.R. Stump, J. Huston, H.L. Lai, P. Nadolsky and W.K. Tung, JHEP 0207 (2002) 012